基于含氟改性笼状倍半硅氧烷一步法制备透明超疏水涂层

徐亚洲[a]，何瑾馨[a,b]，朱卫彪[a]，董霞[a,c]，赵强强[a,b]

（东华大学 a.化学化工与生物工程学院 b.纺织面料技术教育部重点实验室 c.国家染整工程技术研究中心，上海 201620）

摘要：目的 为了研究出一种在光滑镜面基材上大面积制备透明耐用的超疏水涂层，需要克服当前超疏水涂层存在的理化稳定性差、光学透明度不高以及制备繁琐、难以大面积实施等问题。**方法** 通过向聚氨酯丙烯酸酯疏水性光固化树脂体系中引入含氟低表面能改性的笼状倍半硅氧烷（POSS），结合喷涂法和相分离法在聚碳酸酯（PC）表面制备了一种超疏水光固化涂层。探究了低表面能改性 POSS 的掺杂量和乙醇添加量对构筑超疏水涂层的影响。**结果** 当 POSS-SH-DFMA$_7$的掺杂量为树脂含量的 40%、乙醇的添加量为溶剂 THF 的 25%时，涂层表现出优异的超疏水特性，静态水接触角和滑动角分别可达到 156.92°和 3.24°；良好的光学透明性，光线透过率为 85.63%；可靠的机械稳定性，承受 6 h 的水滴冲击后依然保持超疏水特性；稳定的耐候和耐化学性，经历户外环境和不同 pH 值化学试剂的侵蚀后仍可保持涂层原有的润湿性能。**结论** 在光固化树脂体系中引入一定量的含氟单体改性 POSS 结合乙醇的作用可以一步法制备出透明、理化性能稳定的超疏水涂层。

关键词：POSS；超疏水涂层；透明；耐用；喷涂；相分离；紫外光固化

中图分类号：TG174；TB34　**文献标识码：**A　**文章编号：**1001-3660(2022)10-0336-08

DOI：10.16490/j.cnki.issn.1001-3660.2022.10.036

Transparent Superhydrophobic Coating Prepared by One-step Method Based on Fluorinated Cage-like Sesimiloxane

XU Ya-zhou[a], HE Jin-xin[a,b], ZHU Wei-biao[a], DONG Xia[a,c], ZHAO Qiang-qiang[a,b]

(a. School of Chemistry, Chemical Engineering and Biotechnology, b. Key Lab of Textile Science & Technology, Ministry of Education, c. National Engineering Research Center for Dyeing and Finishing of Textiles, Donghua University, Shanghai 201620, China)

ABSTRACT: The coating film-forming method has good application prospects in the preparation of transparent superhydrophobic coatings due to its simple process, good repeatability and low equipment requirements. However, the nanofillers in the

收稿日期：2021–09–22；**修订日期：**2022–01–22

Received：2021-09-22；**Revised：**2022-01-22

基金项目：国家重点研发计划项目（2017YFB0309100）

Fund：Supported by the National Key Technologies R & D Program of China (2017YFB0309100)

作者简介：徐亚洲（1997—），男，硕士研究生，主要研究方向为功能性聚合物材料。

Biography：XU Ya-zhou (1997-), Male, Postgraduate, Research focus: functional polymer material.

通讯作者：何瑾馨（1959—），男，博士，教授，主要研究方向为纺织化学与染整工程。

Corresponding author：HE Jin-xin (1959-), Male, Doctor, Professor, Research focus: textile chemistry and dyeing & finishing engineering.

引文格式：徐亚洲，何瑾馨，朱卫彪，等. 基于含氟改性笼状倍半硅氧烷一步法制备透明超疏水涂层[J]. 表面技术, 2022, 51(10): 336-343.

XU Ya-zhou, HE Jin-xin, ZHU Wei-biao, et al. Transparent Superhydrophobic Coating Prepared by One-step Method Based on Fluorinated Cage-like Sesimiloxane[J]. Surface Technology, 2022, 51(10): 336-343.

existing coating film-forming methods generally have defects such as easy aggregation and poor durability. POSS is an organic-inorganic hybrid with a special cage-like structure. Compared with ordinary nanofillers, POSS has the characteristics of monodispersity and flexible functional modification. At present, most of the researches on POSS in the field of superhydrophobic coatings are based on rough substrate surfaces, but few researches have been done in the field of mirror-transparent optics. Therefore, the purpose of this study is to select POSS as a nanofiller and use a one-step coating film-forming method to construct a large-area transparent and durable superhydrophobic coating on a mirror substrate.

In this study, an intermediate POSS-SH_8 was synthesized from octavinyl POSS and ethanedithiol based on a two-step thiol-ene click chemistry reaction. Then, POSS-SH_8 and dodecafluoroheptyl methacrylate monomer were used as reactants to obtain low surface energy modified product POSS-SH-$DFMA_7$ through photoreaction. The effects of the doping mass fraction of F-POSS and the volume fraction of ethanol addition on the construction of superhydrophobic coatings were explored. The preparation of spraying prefabricated liquid was as follows: F-POSS with different mass fractions was blended in resin prepolymer. Resin prepolymer was composed of a mixture of hydrophobic photocurable resin (Changxing 6145-100) and diluent HDDA at 4∶1. After the prepolymer was evenly mixed, the dilution solvent THF was added to the system at a dilution ratio of 1∶20. It was dispersed uniformly in a stirrer and an ultrasonic shaker successively. In order to obtain the rough micro-nano composite structure on the smooth substrate surface, the method of spraying combined with non-solvent induced phase separation was adopted in this study. Different volume fractions of non-solvent ethanol were added to the above system to obtain a series of spraying prefabricated liquids. Next, the prefabricated solution was transferred to the surface of the smooth substrate by spraying and the coating was air-dried at room temperature. Finally, the air-dried coatings were cured in a UV curing apparatus under N_2 atmosphere for 5 minutes. The chemical composition of the main substances in the obtained samples was analyzed by infrared spectrum curve. The static water contact angle and dynamic rolling angle of the coatings were recorded by contact angle analysis and self-made rolling angle measuring instrument to characterize the hydrophobicity of the coatings. The surface topography and roughness of the composite coatings with different rough structures were investigated by scanning electron microscopy and three-dimensional ultra-depth-of-field microscopy. The transmittance of the coatings was measured by a UV spectrophotometer to characterize the transmittance of the coating. A self-made device was used to set water droplets to be released at a uniform rate of 2 drops per second at a height of 30 cm. The hydrophobic property retention curve of the coatings at different times were obtained to characterize the mechanical stability of the coating. The three superhydrophobic coatings were placed in an outdoor open-air environment, and their contact angle changes were recorded every 3 days to evaluate their weatherability. In addition, the above three coatings were soaked in HCl and NaOH solutions with pH values of 1 to 14 for 24 hours. And the contact angle curves of each coating at different pH values were recorded to compare their resistance to reagents.

The research results show that the coating exhibits excellent superhydrophobic properties when the doping mass fraction of POSS-SH-$DFMA_7$ is 40% of the resin content and the addition volume fraction of ethanol is 25%. The static water contact angle and sliding angle can reach 156.92° and 3.24°, respectively. In addition, the superhydrophobic coating prepared under the optimal process conditions also has good optical transparency and its light transmittance is 85.63%. The coating still maintains superhydrophobic property after being impacted by water droplets for 6 hours, indicating its mechanical stability. Not only that, the original wetting property of the coating can still be maintained after experiencing various outdoor environments and the erosion of chemical agents with different pH values. Therefore, the introduction of a certain amount of fluorine-containing monomer to modify the POSS combined with the phase separation of ethanol into the photocurable resin system can prepare a large-area transparent and superhydrophobic coating with stable physical and chemical properties in one step.

KEY WORDS: POSS; superhydrophobic coating; transparent; durable; spraying; phase separation; UV curing

超疏水表面因为自身独特的润湿性能，已经在越来越多的领域得到广泛应用，如防污自清洁[1-2]、减阻[3-4]、防覆冰[5-6]、油/水分离[7-8]等。最早科学家们受自然界中“荷叶效应”[9]的启发，于 2002 年首次提出了呈现这种大接触角和低附着力是由于表面微纳复合结构协同作用的观点，为之后超疏水表面的模型构建提供了理论基础。目前，制备超疏水表面的构筑方法主要分为两大类——自上而下[10]和自下而上[11]，自上而下法包括模板法[12]、等离子体刻蚀法[13]、印刷法[14]等，自下而上法包括化学沉积法[15]、相分离法[16]、溶胶-凝胶法[17]、喷涂法[18]等。虽然方法纷杂多样，但构造原理都是从降低表面能和提高表面粗糙度这 2 个角度出发。

近些年来，随着超疏水技术在人们生产生活中扮演的角色愈发重要，涂层技术的研究一直在不断革新，从对超疏水基础结构的研究发展到将功能化纳米

粒子低牢度化附着于表面，再到超疏水成分与整体涂层形成均一稳定的连结体系。虽然很多研究已经在超疏水表面的创新性构造方面取得了重大进步，但是真正能规模化生产的产品却少之又少。现阶段，构筑超疏水表面能常使用的低表面能材料主要为长链全氟硅烷[19]、含氟丙烯酸酯[20]和氟硅共聚物[21]，结合纳米粒子的添加形成低表面能的粗糙化表面。但是如何提升纳米粒子与聚合物的有效键合，以及如何改善改性纳米粒子与基材表面的稳定黏附与耐久性始终是一个难点。而且对于一些透明[22]、光滑的基材，如何在不影响透光率的基础上使其具备良好的各项应用性能，是目前透明超疏水涂层领域的一大难题。

为了解决以上问题，本研究采用笼状低聚倍半硅氧烷（POSS[23]）作为粗糙度构建的纳米材料，因为其本身天然的尺度优势（2~5 nm）以及独特的分子内化结构，8 个顶点处的 Si 原子可以通过化学反应连接各种反应性或非反应性基团。因此可以通过巯基-烯点击化学反应[24]将含氟单体引入到 POSS 中，得到的产物不仅具备低表面能特性，还可以参与多层次粗糙结构的构建。另外，由于 POSS 本身具备良好的溶解性、尺寸稳定性和热稳定性等优点，涂层的各项应用性能会随着 POSS 的加入得到显著提升。所以本研究采取将改性纳米 POSS 与光固化树脂[25]（成膜速度快，与基材附着力强）混合，采用一步喷涂法结合相分离法，在聚碳酸酯[26]表面制备出了操作简便、可大规模实施的超疏水涂层。该涂层在不影响基材本身光学透明性的同时还具备良好的机械和化学稳定性。该研究可以为超疏水涂层的大面积生产以及在透明光学领域的大范围应用提供参考。

1　试验

1.1　八乙烯基 POSS 的疏水改性

1.1.1　八乙烯基 POSS 的巯基化

在吴城峰等[27]提出的 POSS-SH_8 合成方法的研究基础上，先对八乙烯基 POSS 进行巯基化处理，得到了 POSS-SH_8。然后利用巯基-烯点击反应对 POSS-SH_8 进行氟烷基改性。

1.1.2　巯基 POSS 的氟烷基化

A 液：将 5.6 g 甲基丙烯酸十二氟庚酯（DFMA）和 0.06 g 光引发剂 I907 溶于 20 mL 无水 THF 中，并且用锡箔纸将其裹好作避光处理。B 液：称量 2.77 g POSS-SH_8 溶于 20 mL 无水 THF 中。整个反应体系是在充满干燥 N_2 的氛围下进行。A 液通过恒压漏斗以 20 mL/h 的恒定速度滴入装有 B 液的平底石英单口烧瓶中，待 A 液滴加完后，在紫外灯下继续曝光搅拌反应 6 h。用聚四氟乙烯注射器滤膜滤去反应后溶液中的不溶物，然后旋转蒸馏除去部分 THF 溶剂。向剩余溶液内加入一定量的无水乙醇后，使用离心机高速离心，得到白色固体物质。接着，使用无水乙醇反复冲洗白色固体物质 5~8 次。最后在 50 ℃的真空干燥烘箱放置 36 h，完全去除溶剂后，得到目标产物 POSS-SH-$DFMA_7$。

1.2　涂层的制备

先将 0.05 g 疏水性树脂与稀释剂 HDDA 混合均匀后（疏水性树脂：HDDA=4∶1），再加入混合树脂质量分数为 2%的光引发剂（I907），以上体系混合均匀后将其加入到 5 mL 的 THF 中。室温下，在转速为 800 r/min 的条件下磁力搅拌 2 h，形成均匀的树脂溶液。然后将不同质量分数的 POSS-SH-$DFMA_7$（10%、20%、30%、40%、50%）（占树脂添加量）和不同体积分数的乙醇（15%、25%、35%、45%、55%）（占 THF 添加量）分别先后加入到溶液中，先在超声波震荡装置中超声分散 1 h，然后室温下磁力搅拌 24 h。

1.3　树脂的喷涂与固化

在喷枪口径为 1.0 mm、流速为 0.25 mL/s、压缩气压为 0.6 MPa 的设置下进行喷涂，基材距离喷枪喷嘴 25~27 cm，移动速度为 3 cm/s，自上而下进行 S 型喷涂。将自然晾干的涂层试样放入紫外光固化仪中，紫外光源是 1 000 W 的高压汞灯，基材距离紫外灯源 28~30 cm，在 N_2 氛围下固化 5 min。

1.4　表征与性能测试

采用傅里叶变温红外光谱仪记录 FTIR 光谱，分析所得样品中主要物质的化学组成。静态水接触角（WCA）使用座滴法通过在样品涂层表面滴加 5 滴 5 μL 的液滴取其平均值。通过扫描电子显微镜和三维超景深显微镜，研究不同粗糙结构复合涂层的表面形貌和粗糙度。采用紫外分光光度计测量涂层的透光率，测试范围 380~800 nm。

涂层机械稳定性测试：采用自制装置，水滴以 2 滴/s 的速率在高度为 30 cm 处匀速释放，测定不同时间下涂层表面的静态接触角。

涂层耐候性：将 3 种超疏水涂层置于户外露天的环境中，每隔 3 d 记录 1 次它们的接触角变化。

化学稳定性测试：将 3 种超疏水涂层用 pH 值为 1~14 的 HCl 和 NaOH 溶液浸没 24 h，记录各个 pH 值下不同涂层的接触角。

2　结果与讨论

2.1　POSS-SH_8 和 POSS-SH-$DFMA_7$ 的结构分析

POSS-SH_8 合成前后主要物质的红外光谱图如图 1a 所示。在八乙烯基 POSS 中，1 604 cm^{-1} 处为

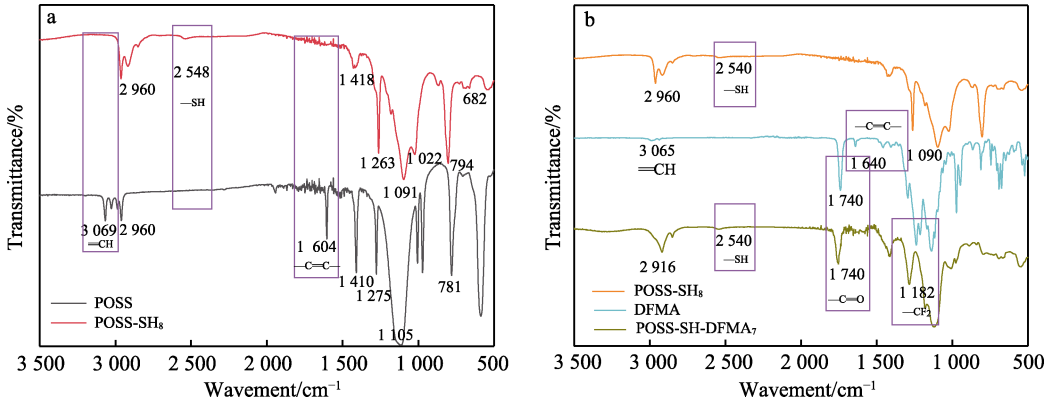

图 1　POSS 巯基化前后（a）及巯基 POSS 氟烷基化前后主要物质的红外光谱图（b）

Fig.1　FTIR spectra of main substances before and after mercaptosylation of POSS (a); FTIR spectra of main substances before and after fluoralkylation of sulfhydryl POSS (b)

—C═C—的伸缩振动特征峰，3 069 cm^{-1} 处为 H_2C═CH—上的 C—H 键的伸缩振动特征峰，而在 POSS-SH_8 中这 2 个特征峰消失了。在新产物中出现了 2 548 cm^{-1} 处的—SH 键的伸缩振动特征峰，1 022 cm^{-1} 处以及 682 cm^{-1} 处 C—S 键的特征振动峰。这些特征峰的消失与出现证明了原八乙烯基 POSS 中的碳碳双键与巯基发生了加成反应，生成了目标产物 POSS-SH_8。POSS-SH-$DFMA_7$ 合成前后主要物质的红外光谱图如图 1b 所示。对比 2 种反应物和 1 种生成产物的红外光谱图，可以发现，在发生巯基-烯点击反应后，生成物中碳碳双键的特征吸收峰消失了，说明含氟丙烯酸酯单体反应完全；在 2 540 cm^{-1} 处生成物相较于反应物 POSS-SH_8 的 S—H 键伸缩振动吸收峰有明显的减弱，说明反应物中部分巯基参与了反应；1 182 cm^{-1} 处的碳氟键和 1 090 cm^{-1} 处的硅氧键特征峰都在生成物中出现了。所以通过以上的分析可以确定 POSS-SH-$DFMA_7$ 被成功合成。

2.2　POSS-SH-$DFMA_7$ 和乙醇的添加量对涂层润湿性能的影响

原 PC 基材的接触角为 76.19°，滚动角大于 90°。纯聚氨酯丙烯酸酯涂层已经达到疏水效果，接触角为 92.78°。为了进一步提升涂层的疏水性能，通过加入改性过的含氟链段改性纳米 POSS 来降低表面能和提升表面粗糙度。根据图 2，纳米 POSS-SH-$DFMA_7$ 的添加量为 20%时，涂层展现出最好的疏水性，θ_{WCA} 为 127°，滚动角为 17°。为了研究乙醇的添加量对涂层疏水性的影响，将 POSS-SH-$DFMA_7$ 的添加量初步确定为 20%，探究不同乙醇添加量对疏水涂层接触角和滚动角的变化。

如图 3 所示，在 POSS-SH-$DFMA_7$ 添加量为 20%的涂层配方体系中，当乙醇的添加量为 25%时，涂层 θ_{WCA} 的达到了 139°，此时的 θ_{SA} 最小，为 11°。由于 THF 的挥发性大于乙醇，溶剂 THF 挥发后，涂层里剩下未挥发的不良溶剂乙醇，纳米 POSS 在乙醇诱导聚集的作用下，慢慢凝聚成尺寸更大的颗粒。当体系中乙醇添加量小于 25%时，期间的粗糙微结构数量虽然很多，但是由于乙醇量较少导致聚集程度不

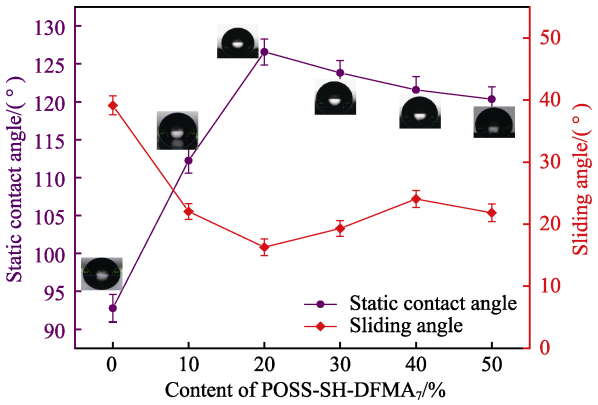

图 2　POSS-SH-$DFMA_7$ 含量对涂层表面润湿性能的影响

Fig.2 Influence of POSS-SH-$DFMA_7$ content on wettability of coating surface

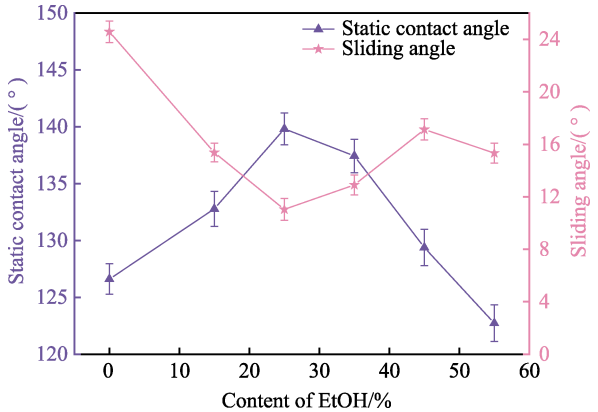

图 3　POSS-SH-$DFMA_7$ 添加量为 20%时乙醇的添加量对涂层润湿性能的影响

Fig.3 Influence of ethanol addition amount of POSS-SH-$DFMA_7$ at 20% on wettability of coating

够，颗粒多以纳米级结构为主，难以托举起水滴，因此该过程中涂层的接触角随乙醇量的增加而变大。当加入的乙醇量为 45%时，聚集达到临界状态，粗糙度达到最大。进一步提升乙醇的添加量，就会促使大颗粒形成，导致表面微结构数量减少，疏水性能下降。

由于 POSS-SH-DFMA$_7$添加量为 20%时无法使涂层具备超疏水特性。于是分别探究了低表面能纳米 POSS 添加量为 30%、40%、50%的情况下乙醇的最佳添加比例。如图 4a 所示，当 POSS-SH-DFMA$_7$的添加量为 30%时，乙醇添加量为 35%，此时疏水效果最佳，θ_{WCA}增大到 151°，θ_{SA}降低至 8°左右，已经达到超疏水效果。如图 4b 所示，纳米 POSS-SH-DFMA$_7$的添加量为 40%、乙醇的添加量为 25%时，构造出了静态水接触角达 157°、滚动角小到 3.3°的超疏水表面。如图 4c 所示，低表面能纳米尺寸粒子添加量为 50%时，涂层疏水性的变化趋势与 POSS-SH-DFMA$_7$添加量为 40%时大体一致。乙醇添加量为 25%时，涂层的疏水性能最佳，静态水接触角可达 161°，滚动角更是小至 1.8°。

2.3　POSS-SH-DFMA$_7$ 光固化涂层表面形貌分析

采用 SEM 扫描电子显微镜和三维超景深显微镜分别对 POSS-SH-DFMA$_7$添加量为 30%、40%、50%最佳疏水效果涂层进行表面形貌和粗糙度表征，结果如图 5 所示。从图 5 可以看出，随着纳米 POSS-SH-DFMA$_7$ 添加量的增加，涂层表面形成的微米团簇变得越来越多，间隙越来越小。由于团簇是微纳复合结构，这种分级结构可以捕获大量空气，致使涂层表面和水滴之间可以产生一层“气垫”，这层“气垫”极大地减少了水滴与固体表面的接触面积，因此疏水性能得到提升。粗糙度在 3D 超景深图像中体现为凸起结构的高度和密度。由图 5 三维超景深显微结果可知，在乙醇相分离的作用下，粗糙度随纳米 POSS-SH-DFMA$_7$ 添加量的增加而变得越来越大，平均粗糙度 *Ra* 分别为 1.87、4.43、5.54 μm。这与涂层 SEM 图所反映出的信息一致。

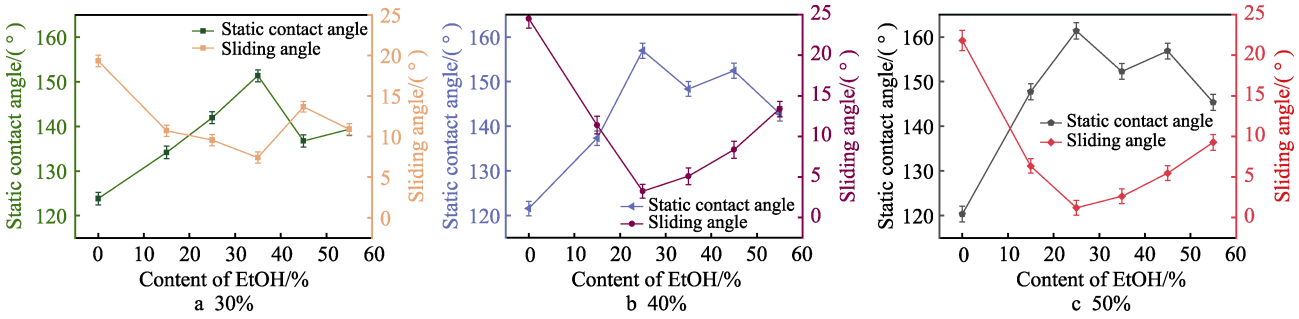

图 4　POSS-SH-DFMA$_7$添加量分别为 30%、40%和 50%时乙醇的添加量对涂层润湿性能的影响

Fig.4 Influence of ethanol addition amount of POSS-SH-DFMA$_7$ at 30%, 40% and 50% on wettability of coating

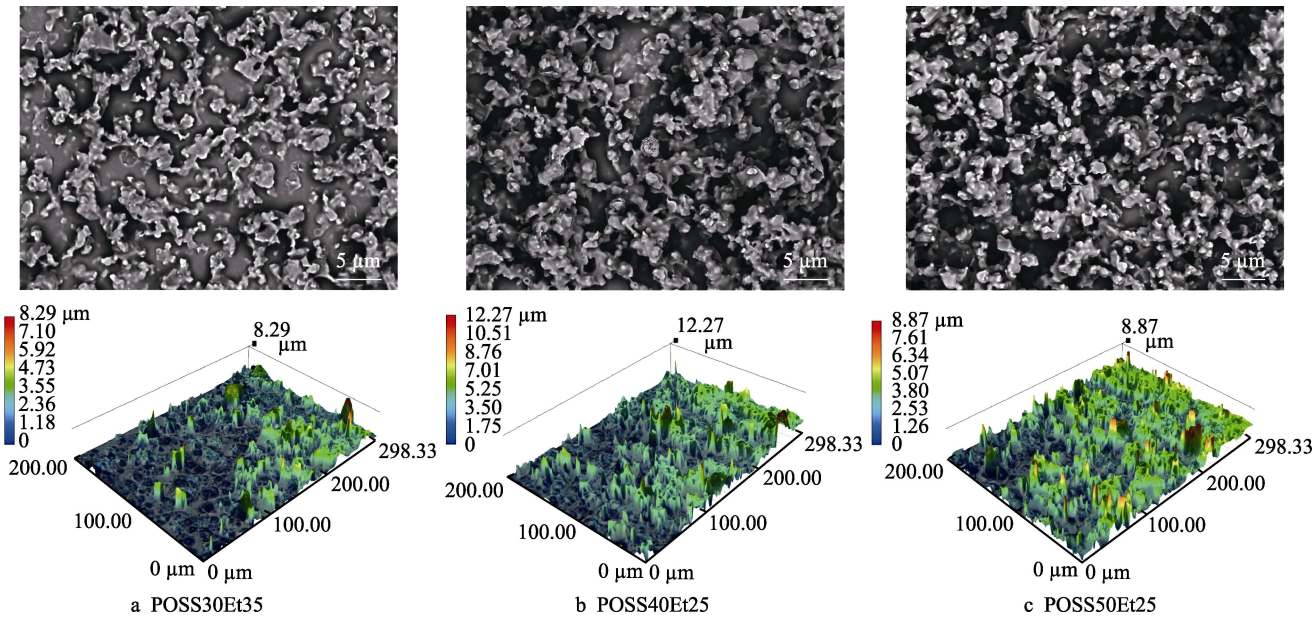

图 5　POSS30Et35、POSS40Et25 和 POSS50Et25 涂层试样的表观形貌和表观粗糙度

Fig.5　The apparent morphologies and roughness of the coated specimens POSS30Et35, POSS40Et25 and POSS50Et25

2.4　涂层透光性能测试

通过紫外分光光度计测试 PC 空白试样和 POSS30Et35、POSS40Et25、POSS50Et25 超疏水涂层的透光率，其透光率曲线如图 6 所示。从透光率曲线可以看出，在 450~780 nm 波段范围内 PC 空白试样的平均透光率为 89.76%，涂层 POSS30Et35 的平均透光率为 86.12%，涂层 POSS40Et25 的平均透光率为 83.63%，涂层 POSS50Et25 的平均透光率为 77.37%。在乙醇的相分离作用下，3 种超疏水涂层的透明性是随着纳米颗粒添加量的增加呈现出下降的趋势。光的散射和折射是影响涂层光线透过率的主要因素。

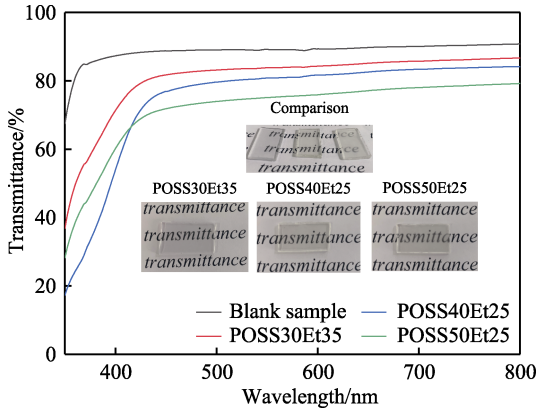

图 6　空白试样、POSS30Et35、POSS40Et25 和 POSS50Et25 样品的涂层透过率曲线

Fig.6 Coating transmittance curves of the blank sample, POSS30Et35, POSS40Et25 and POSS50Et25

2.5　涂层的机械稳定性测试

使用如图 7a 所示的水滴冲击自制设备，进行超疏水涂层机械稳定性能的表征。以每秒 2 滴的速率向涂层表面释放液滴，每隔 0.5 h 记录各涂层的接触角变化，如图 7b 所示。在经过水滴冲击 4 h 后，涂层 POSS30Et35 的超疏水性消失。而另外 2 个涂层体系中，由于纳米粒子更多且分布更均匀，即使在水滴冲击 6 h 后，依然维持着良好的超疏水特性。其中涂层 POSS40Et25 的接触角的下降幅度最小，说明其耐水滴冲击性能最优异，机械稳定性最好。

2.6　涂层的耐候和化学稳定性能测试

图 8a 是 3 种超疏水涂层在户外环境中的耐候测试结果，在相同的测试周期中，3 种涂层的接触角都

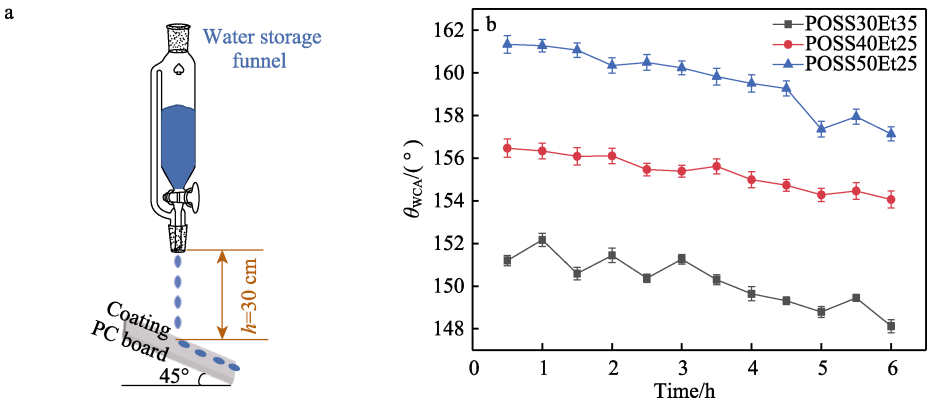

图 7　耐水滴冲击测试装置图（a）及 3 种涂层表面在 6 h 水滴的持续冲击下接触角值的变化（b）

Fig.7 Diagram of droplet impact resistance test device (a); changes in contact angle values of the three coating surfaces under 6-hour continuous impact of water droplets (b)

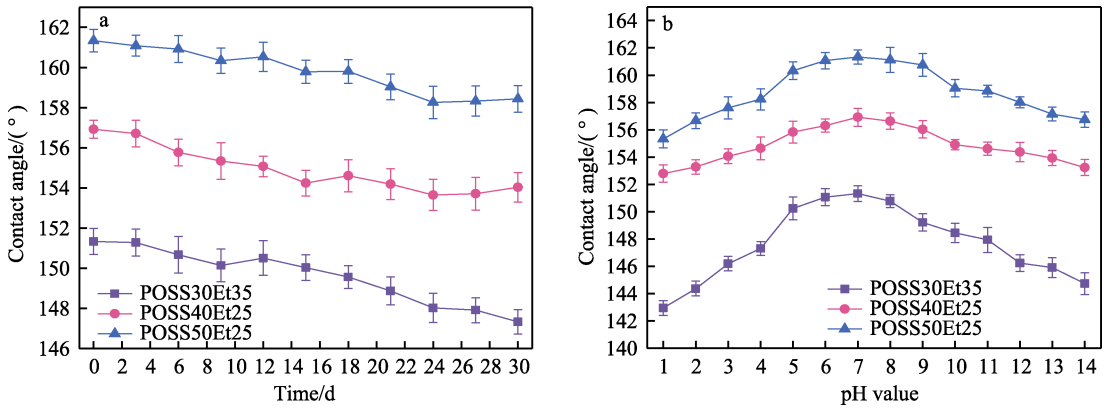

图 8　3 种超疏水涂层在户外环境中的耐气候测试（a）及不同 pH 值下的化学稳定性测试（b）

Fig.8Weather resistance test of three superhydrophobic coatings in an outdoor environment (a); Chemical stability tests of three superhydrophobic coatings at different pH values (b)

呈现出了一定的下降趋势，其中涂层 POSS40Et25 的下降幅度最小，说明该涂层的耐候性能最稳定。图 8b 是 3 种超疏水涂层的化学稳定性测试结果。3 种超疏水涂层对不同 pH 值范围的溶液展现出不同的化学稳定性，根据图示曲线的起伏程度，可发现涂层 POSS40Et25 对不同溶剂的适应力更强，化学稳定性最佳。相较于涂层 POSS30Et35，涂层 POSS40Et25 具有更致密的粗糙结构和更高的表面起伏，不管是雨水还是酸碱溶液，与空气的接触面积大，不易与涂层内部直接接触，受侵蚀的程度更小，疏水性能的保持能力更好。而涂层 POSS40Et25 比涂层 POSS50Et25 的耐候和化学稳定性更优，主要归因于前者涂层体系中纳米 POSS 的添加量适度，相分离后的粗糙结构与光固化树脂之间存在的有效连接趋向于体系的饱和值。另外，在本试验条件下制备的涂层对涉及酸雨的实际应用效果更好。

3 结论

本文选取一步喷涂相分离法结合紫外光固化技术作为制备超疏水涂层的方法。采用聚氨酯疏水改性丙烯酸酯作为树脂基体，HDDA 为预聚体稀释剂，低表面能的 POSS-SH-DFMA$_7$ 为纳米填料，THF 为溶剂，乙醇为不良溶剂。综合探究分析后，得出以下结论：当纳米 POSS-SH-DFMA$_7$ 添加量为树脂的 40%，不良溶剂乙醇添加量为 THF 的 25%时，涂层的超疏水效果优异，θ_{WCA} 值可达到 156.92°，滚动角小至 3.24°，而且涂层的各项应用性能更贴合使用需求，比如高达 85.63%的涂层透明度、经受长时间水滴冲击测试后可靠的涂层黏结力、多元环境长期作用后优异的涂层耐候性能以及不同 pH 值化学试剂侵蚀后稳定的涂层耐化学性能。

参考文献：

[1] CHEN Jian-yu, YUAN Lu-han, SHI Chu, et al. Nature-Inspired Hierarchical Protrusion Structure Construction for Washable and Wear-Resistant Superhydrophobic Textiles with Self-Cleaning Ability[J]. ACS Applied Materials & Interfaces, 2021, 13(15): 18142-18151.

[2] QIN Li-guo, HAFEZI M, YANG Hao, et al. Constructing a Dual-Function Surface by Microcasting and Nanospraying for Efficient Drag Reduction and Potential Antifouling Capabilities[J]. Micromachines, 2019, 10(7): 490.

[3] BUSCH J, BARTHLOTT W, BREDE M, et al. Bionics and Green Technology in Maritime Shipping: An Assessment of the Effect of Salvinia Air-Layer Hull Coatings for Drag and Fuel Reduction[J]. Philosophical Transactions Series A, Mathematical, Physical, and Engineering Sciences, 2019, 377(2138): 20180263.

[4] YAO Chang-zhuang, ZHANG Jing-jing, XUE Zi-han, et al. Bioinspired Cavity Regulation on Superhydrophobic Spheres for Drag Reduction in an Aqueous Medium[J]. ACS Applied Materials & Interfaces, 2021, 13(3): 4796-4803.

[5] SHEN Yi-zhou, WANG Guan-yu, TAO Jie, et al. Anti-Icing Performance of Superhydrophobic Texture Surfaces Depending on Reference Environments[J]. Advanced Materials Interfaces, 2017, 4(22): 1700836.

[6] WANG Nan, XIONG Dang-sheng, DENG Ya-ling, et al. Mechanically Robust Superhydrophobic Steel Surface with Anti-Icing, UV-Durability, and Corrosion Resistance Properties[J]. ACS Applied Materials & Interfaces, 2015, 7(11): 6260-6272.

[7] ZHANG Ji-xi, ZHANG Li-gui, GONG Xiao. Design and Fabrication of Polydopamine Based Superhydrophobic Fabrics for Efficient Oil-Water Separation[J]. Soft Matter, 2021, 17(27): 6542-6551.

[8] LUO Wen-jun, SUN Da-wei, CHEN Shu-sheng, et al. Robust Microcapsules with Durable Superhydrophobicity and Superoleophilicity for Efficient Oil-Water Separation[J]. ACS Applied Materials & Interfaces, 2020, 12(51): 57547-57559.

[9] YAMAMOTO M, NISHIKAWA N, MAYAMA H, et al. Theoretical Explanation of the Lotus Effect: Superhydrophobic Property Changes by Removal of Nanostructures from the Surface of a Lotus Leaf[J]. Langmuir: The ACS Journal of Surfaces and Colloids, 2015, 31(26): 7355-7363.

[10] WANG Ming-fang, RAGHUNATHAN N, ZIAIE B. A Nonlithographic Top-down Electrochemical Approach for Creating Hierarchical (Micro–Nano) Superhydrophobic Silicon Surfaces[J]. Langmuir, 2007, 23(5): 2300-2303.

[11] ZOU Rui-qing, WANG Jian, TANG Jian-bin, et al. Directionally Guided Droplets on a Modular Bottom-up Anisotropic Locally Ordered Nickel Nanocone Superhydrophobic Surface[J]. ACS Applied Materials & Interfaces, 2021, 13(11): 13848-13860.

[12] GONG Ding-wei, LONG Jiang-you, JIANG Da-fa, et al. Robust and Stable Transparent Superhydrophobic Polydimethylsiloxane Films by Duplicating via a Femtosecond Laser-Ablated Template[J]. ACS Applied Materials & Interfaces, 2016, 8(27): 17511-17518.

[13] NGUYEN-TRI P, ALTIPARMAK F, NGUYEN N, et al. Robust Superhydrophobic Cotton Fibers Prepared by Simple Dip-Coating Approach Using Chemical and Plasma-Etching Pretreatments[J]. ACS Omega, 2019, 4(4): 7829-7837.

[14] ZHAO Yuan-yuan, LIU Yang, XU Qian-feng, et al. Catalytic, Self-Cleaning Surface with Stable Superhydrophobic Properties: Printed Polydimethylsiloxane (PDMS) Arrays Embedded with TiO_2 Nanoparticles[J]. ACS Applied Materials & Interfaces, 2015, 7(4): 2632-2640.

[15] ZHUANG Ao-yun, LIAO Rui-jin, LU Yao, et al. Trans-

forming a Simple Commercial Glue into Highly Robust Superhydrophobic Surfaces via Aerosol-Assisted Chemical Vapor Deposition[J]. ACS Applied Materials & Interfaces, 2017, 9(48): 42327-42335.

[16] BIRIA S, HOSEIN I D. Superhydrophobic Microporous Substrates via Photocuring: Coupling Optical Pattern Formation to Phase Separation for Process-Tunable Pore Architectures[J]. ACS Applied Materials & Interfaces, 2018, 10(3): 3094-3105.

[17] SU Xiao-jing, LI Hong-qiang, LAI Xue-jun, et al. Vapor-Liquid Sol-Gel Approach to Fabricating Highly Durable and Robust Superhydrophobic Polydimethylsiloxane@ Silica Surface on Polyester Textile for Oil-Water Separation[J]. ACS Applied Materials & Interfaces, 2017, 9(33): 28089-28099.

[18] SPARKS B J, HOFF E F T, XIONG Li, et al. Superhydrophobic Hybrid Inorganic-Organic Thiol-Ene Surfaces Fabricated via Spray-Deposition and Photopolymerization [J]. ACS Applied Materials & Interfaces, 2013, 5(5): 1811-1817.

[19] ZHU Qun-yan, TENG Fei, WANG Zhong-shun, et al. Superhydrophobic Glass Substrates Coated with Fluorosilane-Coated Silica Nanoparticles and Silver Nanoparticles for Surface-Assisted Laser Desorption/Ionization Mass Spectrometry[J]. ACS Applied Nano Materials, 2019, 2(6): 3813-3818.

[20] ITO S, KANEKO S, YUN C M, et al. Investigation of Fluorinated (Meth)Acrylate Monomers and Macromonomers Suitable for a Hydroxy-Containing Acrylate Monomer in UV Nanoimprinting[J]. Langmuir: The ACS Journal of Surfaces and Colloids, 2014, 30(24): 7127-7133.

[21] ZHANG Wei, ZHENG Ying, ORSINI L, et al. More Fluorous Surface Modifier Makes it less Oleophobic: Fluorinated Siloxane Copolymer/PDMS Coatings[J]. Langmuir: The ACS Journal of Surfaces and Colloids, 2010, 26(8): 5848-5855.

[22] KE Chong, ZHANG Chen-hua, WU Xin-guo, et al. Highly Transparent and Robust Superhydrophobic Coatings Fabricated via a Facile Sol-Gel Process[J]. Thin Solid Films, 2021, 723: 138583.

[23] XUE Yu-hua, LIU Yong, LU Fan, et al. Functionalization of Graphene Oxide with Polyhedral Oligomeric Silsesquioxane (POSS) for Multifunctional Applications[J]. The Journal of Physical Chemistry Letters, 2012, 3(12): 1607-1612.

[24] ZHANG Pan, WANG Qiang, SHEN Jin-song, et al. Enzymatic Thiol-Ene Click Reaction: An Eco-Friendly Approach for MPEGMA-Grafted Modification of Wool Fibers[J]. ACS Sustainable Chemistry & Engineering, 2019, 7(15): 13446-13455.

[25] YU Bin, WANG Xin, XING Wei-yi, et al. UV-Curable Functionalized Graphene Oxide/Polyurethane Acrylate Nanocomposite Coatings with Enhanced Thermal Stability and Mechanical Properties[J]. Industrial & Engineering Chemistry Research, 2012, 51(45): 14629-14636.

[26] SCHULTZ C W, NG C L W, YU Hua-zhong. Superhydrophobic Polydimethylsiloxane via Nanocontact Molding of Solvent Crystallized Polycarbonate: Optimized Fabrication, Mechanistic Investigation, and Application Potential [J]. ACS Applied Materials & Interfaces, 2020, 12(2): 3161-3170.

[27] 吴城锋, 朱卫彪, 何瑾馨, 等. 聚醚改性多面体低聚倍半硅氧烷构筑耐水性亲水防雾涂层[J]. 表面技术, 2020, 49(8): 123-131.
WU Cheng-feng, ZHU Wei-biao, HE Jin-xin, et al. Water Resistant Hydrophilic Anti-Fog Coating Constructed by Polyether Modified Polyhedral Oligosilsesquioxanes[J]. Surface Technology, 2020, 49(8): 123-131.

责任编辑：万长清

（上接第 293 页）

[17] 徐仰涛, 刘志健, 朱珍旭, 等. 铜离子对工业电解液中镍电结晶行为的影响[J]. 中国有色金属学报, 2021, 31(4): 984-994.
XU Yang-tao, LIU Zhi-jian, ZHU Zhen-xu, et al. Effect of Copper Ions on Electrocrystallization Behavior of Nickel in Industrial Electrolyte[J]. The Chinese Journal of Nonferrous Metals, 2021, 31(4): 984-994.

[18] LI Bao-song, MEI Tian-yong, LI Dan-dan, et al. Structural and Corrosion Behavior of Ni-Cu and Ni-Cu/ZrO_2 Composite Coating Electrodeposited from Sulphate-Citrate Bath at Low Cu Concentration with Additives[J]. Journal of Alloys and Compounds, 2019, 804: 192-201.

[19] QIN Li-yuan, LIAN Jian-she, JIANG Qing. Effect of Grain Size on Corrosion Behavior of Electrodeposited Bulk Nanocrystalline Ni[J]. Transactions of Nonferrous Metals Society of China, 2010, 20(1): 82-89.

[20] BOUKHVALOV D W, ZHIDKOV I S, KUKHARENKO A I, et al. Stability of Boron-Doped Graphene/Copper Interface: DFT, XPS and OSEE Studies[J]. Applied Surface Science, 2018, 441: 978-983.

[21] MONACO L, SODHI R N S, PALUMBO G, et al. XPS Study on the Passivity of Coarse-Grained Polycrystalline and Electrodeposited Nanocrystalline Nickel-Iron (NiFe) Alloys[J]. Corrosion Science, 2020, 176: 108902.

责任编辑：彭颋